Dalton Transactions

ROYAL SOCIETY OF CHEMISTRY

PAPER

View Article Online
View Journal | View Issue

Cite this: *Dalton Trans.*, 2021, **50**, 15914

Robust ionic liquid@MOF composite as a versatile superprotonic conductor†

Kiran Taksande, [a,b] Effrosyni Gkaniatsou,[c] Corine Simonnet-Jégat,[c] Carine Livage,[c] Guillaume Maurin, [a] Nathalie Steunou [c] and Sabine Devautour-Vinot *[a]

Received 26th August 2021,
Accepted 22nd October 2021

DOI: 10.1039/d1dt02877d

rsc.li/dalton

A highly performing proton conducting composite was prepared through the impregnation of EMIMCl ionic liquid in the mesoporous MIL-101(Cr)–SO_3H MOF. The resulting EMIMCl@MIL-101(Cr)–SO_3H composite displays high thermal and chemical stability, alongside retention of a high amount of EMIMCl even at temperatures as high as 500 K, as well as under moisture conditions. Remarkably, this composite exhibits outstanding proton conductivity not only at the anhydrous state ($\sigma_{473\ K} = 1.5 \times 10^{-3}$ S cm^{-S}) but also under humidity ($\sigma_{(343\ K/60\%-80\%RH)} \geq 0.10$ S cm^{-1}) conditions. This makes EMIMCl@MIL-101(Cr)–SO_3H a unique candidate to act as a solid state proton conductor for PEMFC applications under versatile conditions.

Introduction

To meet the growing demand of energy along with the urgent reduction of greenhouse gas emission, the development of green and sustainable devices for energy production, distribution, storage and conversion is still challenging.[1] Owing to their high power density combined with negligible emission features, Proton Exchange Membrane Fuel Cells (PEMFC) have been prioritized, with many efforts dedicated to the design and development of efficient proton conductors displaying high proton conductivity and operating over a wide temperature range.[2] In this context, Metal–Organic Frameworks (MOFs) have emerged as new solid-state proton conductors, because of their high modular variability in terms of crystalline structure, pore diameter/shape and chemical functionality.[3–10] Different strategies have been envisaged to optimize the proton conductivity of MOFs by either incorporating intra-framework proton sources through adequate functionalization of their organic or inorganic nodes or by introducing extra-proton carriers in the MOF pores to impart multiple proton pathways. These approaches are categorized as follows: (i) grafting of proton sources onto the MOF framework using Brønsted acidic groups (–SO_3H, –CO_2H, –PO_3H_2 acid-based functions),[11–15] (ii) introduction of proton carriers (NH_4^+, $Me_2NH_2^+$) as counter ions in anionic MOF pores,[16–18] (iii) incorporation of proton transfer agents, *i.e.* guest amphiprotic molecules (non-volatile strong acid molecules,[19–21] polyoxometalates,[22,23] N-heterocyclic compounds,[24–26] ionic liquids[27–42]) in MOF pores or (iv) consideration of defective MOFs or frameworks displaying structural transformations to tune the concentration and mobility of proton carriers.[43,44] This led to the development of two categories of MOF-based proton conductors for PEMFC applications, *i.e.* anhydrous or water-mediated conductors operating at intermediate (373 K < T < 473 K) or low (T < 373 K) temperatures respectively. Notably, proton conducting MOFs achieving high conductivity for both temperature domains have been only rarely reported so far.[16,45] This observation is still valid for other classes of solids and composites typically investigated for this purpose, *i.e.* polyphosphates and hybrid polymer-based membranes.[46–49] We believe that the development of MOF-based composites with versatile superconductor behavior offers an opportunity to address this great challenge.

Ionic Liquids (ILs) are organic salts known as efficient charge transfer agents owing to their low volatility, wide liquid range, good ionic conductivity and high thermal/chemical stability.[50] They have been successfully incorporated in the MOF pores (IL@MOF) for the development of conductors applicable to different fields including Li or Na batteries, redox flow batteries and PEMFC.[27–42,51–53] Regarding proton conducting IL@MOFs, imidazolium based-ILs were mainly explored with the consideration of a variety of counter ions,

[a]*ICGM, University of Montpellier, CNRS, ENSCM, Montpellier, France. E-mail: sabine.devautour-vinot@umontpellier.fr*
[b]*Government of Maharashtra's, Ismail Yusuf College, Jogeshwari(E), Mumbai, Maharashtra 411060, India*
[c]*Institut Lavoisier de Versailles UMR CNRS 8180, Université de Versailles St Quentin en Yvelines, Université Paris Saclay, Versailles, France*

†Electronic supplementary information (ESI) available: Characterization of the pristine sample and composite (SEM-EDX, EA, TGA, FTIR, impedance measurements and water adsorption isotherm). See DOI: 10.1039/d1dt02877d

e.g. halogen,[27,29] sulfonate,[36] dicyanamide[40] and thiocyanate[33] in order to tune their chemical compatibility with the MOF matrices. Incorporation of binary ILs in the MOF pores were also envisaged resulting in Brønsted acid–base buffers shown to introduce both H^+-source and H^+-defect sites promoting the H^+ hopping process.[34,36,37] In these previous works, ILs were mostly impregnated in microporous MOFs, including NH_2-MIL-53(Cr),[27] ZIF-8(Zn),[28] UiO-67(Zr)[29,30] among others,[31–35] while mesoporous MOFs *e.g.* MIL-101(Cr)[36–39] or PCN-777 (Zr)[40] were considered to enable high IL loadings. In comparison with the behavior of the bulk ILs, the proton transport properties of the confined ILs were found to be enhanced as a result of the optimal spatial distribution of ILs within the MOF pores. Notably the MOFs matrices considered so far do not exhibit any relevant intrinsic proton conductivity. Moreover, it is worth noting that ZIF-8(Zn) and UiO-67(Zr) do not exhibit a good chemical stability in aqueous solution and/or water vapor,[54–56] which strongly limits their practical use in PEMFC applications under hydration conditions. As a consequence, these composites were mostly investigated under anhydrous conditions with protonic conductivity reaching 10^{-2} S cm^{-1} at 343 K,[40] while only a very few of them were tested under humid conditions, but restricted to low Relative Humidity level (RH ≈ 25%) to most probably avoid IL leaching and/or MOF degradation. In the latter case, protonic conductivity of range [3×10^{-5}–4×10^{-2} S cm^{-1}] were recorded at $T <$ 353 K.[27–39]

Herein, MOF is aimed to act not only as a host scaffold of IL but also as a source of acidic protons. Therefore, we selected the mesoporous MIL-101(Cr)–SO_3H that combines (i) mesoporous cages to confine a large amount of ILs, (ii) sulfonic acid functionalized terephthalate linkers with Brønsted acid functions able to deliver protons and (iii) an excellent chemical and thermal stability. This sulfonic acid-functionalized MOF was previously shown to exhibit high H^+ conductivity under humid conditions.[14,20,21] Regarding the IL, 1-Ethyl-3-methyl Imidazolium chloride (EMIMCl) was chosen as its loading in the UiO-67(Zr) pores led to attractive proton conductivity performance at the anhydrous state.[29] Remarkably the protonic conductivity of the resulting composite, labelled EMIM@MIL-101-SO_3H, was found to be amongst the highest values reported so far for IL@MOF composites at the anhydrous state ($\sigma_{(473\ K)} = 1.5 \times 10^{-3}$ S cm^{-1}). Decisively, this composite also exhibits an unprecedented protonic conductivity under low/mild humidity conditions ($\sigma > 1.0 \times 10^{-1}$ S cm^{-1} at 343 K for RH = [60%–80%]. This makes EMIM@MIL-101-SO_3H as an optimal versatile superprotonic conductor for future PEMFC applications operating under a variety of working conditions for both mobile and transportation power applications.

Experimental section

Chemical and synthesis

All the chemicals were purchased from commercial sources and used without further purifications.

Synthesis of MIL-101(Cr)–SO_3H

The synthesis of MIL-101(Cr)–SO_3H was performed following the procedure reported previously.[57] 400 mg of Cr $(NO_3)_3 \cdot 9H_2O$ (1 mmol) and 840 mg of 2-sulfoterephthalic acid (3 mmol, BDC-SO_3H) were dissolved in 5 mL of 27 mM tetramethylammonium hydroxide (TMAOH) solution. This reaction mixture was heated in a 15 mL Teflon reactor under autogenous pressure at 463 K for 24 h. After cooling down to room temperature and centrifugation, the solid product was washed three times with water and three times with absolute ethanol. The resulting material was stored in ethanol.

Preparation of EMIM@MIL-101-SO_3H

A saturated solution of 1-Ethyl-3-Methyl Imidazolium Chloride (EMIMCl) was prepared by introducing 6500 mg (44.3 mmol) of EMIMCl in 5 mL of aqueous solution, while the pH was fixed at 3. 900 mg (1 mmol) MIL-101(Cr)–SO_3H was suspended in the EMIMCl saturated solution and stirred magnetically for 24 h at room temperature. The solid was filtered, washed using 4 mL of methanol solution and dried at 373 K for 8 h.

Methods

Powder X-Ray diffraction. The PXRD patterns were collected on a PANalytical X'Pert diffractometer equipped with an X'Celerator detector (λ = 1.5406 Å), with an operating voltage of 40 kV and a beam current of 30 mA.

Nitrogen sorption isotherm. N_2 sorption measurements were performed at 77 K using a Micromeritics, Tristar 3000 analyzer. Samples were out-gassed by heating at 393 K for 16 h under vacuum (<10^{-5} Torr) before N_2 physisorption measurements.

Water sorption isotherm. The water sorption isotherm was measured using a DVS gravimetric sorption system (from surface measurement systems). The apparatus was automatically operated to precisely control the water vapor pressure (0–95 RH%) and temperature (303 K). Prior to adsorption experiments, the samples were dehydrated at 423 K for 8 h under high vacuum (<10^{-6} torr).

FTIR spectroscopy. Infrared spectra were recorded on a FTIR Magna 550 Nicolet spectrophotometer using the technique of pressed KBr pellets at a resolution of 4 cm^{-1}.

Scanning electron microscopy with energy dispersive X-Ray analysis (SEM-EDX). SEM images were recorded on gold coated samples using a JEOL JSM-7001F microscope equipped with an energy-dispersive X-ray (EDX) spectrometer with a X-Max SDD (Silicon Drift Detector) by Oxford.

Elemental analysis (EA). EA was performed using a Flash EA 1112 (Thermofinnigan) apparatus.

Thermogravimetric analysis (TGA) and TGA coupled with mass spectrometry (TGA-MS). TGA-MS measurements were collected on a STA 449 F1 Jupiter – QMS 403D Aëolos Netzsch system, from 298 K to 973 K under heating (q = 2 K min^{-1}) and using 100 mL min^{-1} of an Argon flow. TGA measurements were equally carried out under O_2 flow.

Differential scanning calorimetry (DSC). DSC experiments were carried out using a DSC 1 device from METTLER TOLEDO, in sealed Al-pans (40 mL) under dried N_2 atmosphere (250 mL min^{-1}). The solid was *in situ* heated at 473 K for 2 h, before recording the signal under subsequent cooling (from 373 K to 150 K) and heating (from 150 K to 373 K) using a ramp of 7 K min^{-1}.

Impedance measurements

Impedance measurements were performed on a Broadband Dielectric Spectrometer, Novocontrol alpha analyzer, over a frequency range from 10^{-2} Hz to 1 MHz with an applied *ac* voltage of 20 mV. Measurements were collected on the anhydrous EMIM@MIL-101-SO_3H, after a preliminary *in situ* heating at 473 K for 2 h under nitrogen flow. According to TGA results, the solid is fully dehydrated, while no IL release occurs under these operating conditions. Measurements were equally undertaken on the humidified solid, which was introduced into an Espec Corp. SH-221 incubator, to control the temperature 298 < T (K) < 363 and the relative humidity 40 < RH (%) < 95. The solid was equilibrated for 24 h at given T and RH values, to ensure fixed water content before recording the impedance. The measurements were performed using powders introduced in a home-made sample holder.

Results and discussion

MIL-101(Cr)–SO_3H was synthesized according to the reported procedure[57] and fully characterized by combining Powder X-Ray Diffraction (PXRD), Fourrier-Transform Infra-red (FT-IR), Thermogravimetric Analysis (TGA) and N_2 adsorption. According to the elemental analysis, 68% of the organic linker of the MOF was functionalized by –SO_3H groups (see Table S1†). The EMIM@MIL-101-SO_3H composite was further prepared at room temperature through post-impregnation method, using a saturated solution of EMIMCl (see Experimental details in ESI†). As illustrated in Fig. 1a, the PXRD pattern of the composite displays the characteristic Bragg peaks of MIL-101(Cr)–SO_3H, thereby showing that the crystalline structure of the MOF is preserved upon EMIMCl impregnation. Noteworthy, the lower intensity of the Bragg peaks at low angles for EMIM@MIL-101-SO_3H results from the modification of the electron density in the MOF pores and a disordered distribution of the EMIMCl confined in the mesoporous cages of the MOF,[21,40–42] as previously reported for $CaCl_2$/MIL-101(Cr) and $SrBr_2$/MIL-101(Cr) composites.[58,59]

The SEM images of the EMIM@MIL-101-SO_3H composite showed that the morphology of MOF crystallites is not altered after the IL impregnation (see Fig. S1 and S2†). SEM and

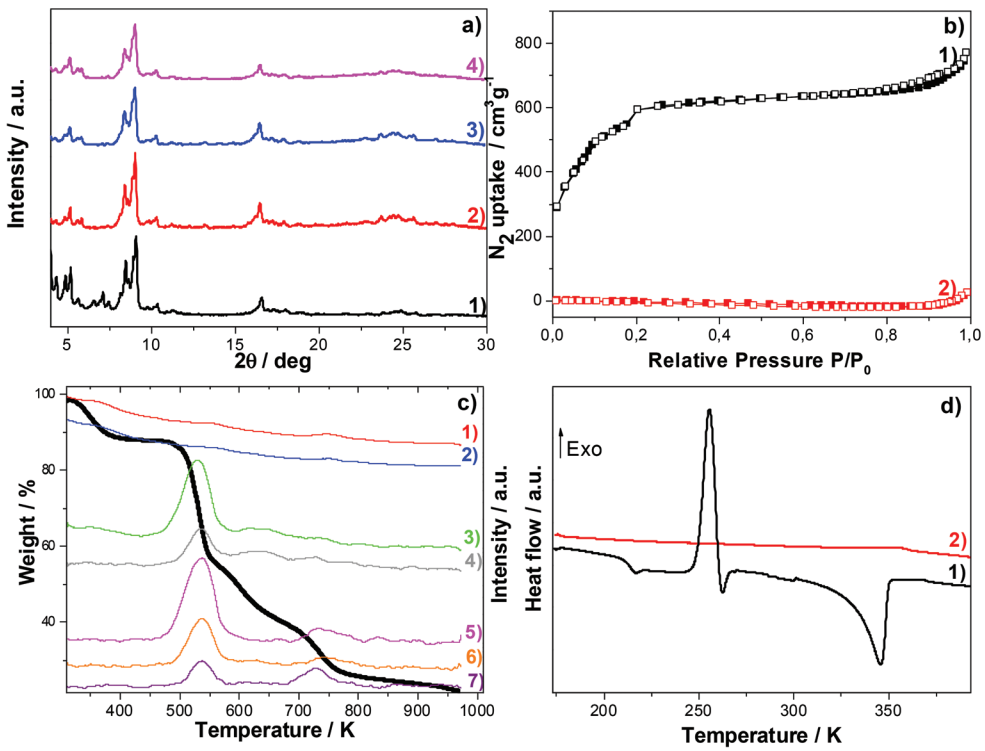

Fig. 1 (a) PXRD patterns of (1) the pristine MIL-101(Cr)–SO_3H, (2) EMIM@MIL-101-SO_3H before conductivity measurements, (3) EMIM@MIL-101-SO_3H after conductivity measurements recorded in the temperature range of 273–473 K and (4) EMIM@MIL-101-SO_3H after conductivity measurements recorded at 363 K and relative humidity (RH) ranging from 35% to 80%, (b) nitrogen sorption isotherms of (1) MIL-101-SO_3H and (2) EMIM@MIL-101-SO_3H: filled and empty symbols correspond to the adsorption and the desorption branches respectively, (c) TGA plot (wt%) of EMIM@MIL-101-SO_3H and the corresponding EGA curves specific to fragments of water and EMIMCl: lines 1, 2, 3, 4, 5, 6 and 7 refer to m/z = 17, 18, 15, 29, 50, 52 and 64 respectively and (d) DSC heating profiles for (1) EMIMCl and (2) EMIM@MIL-101-SO_3H.

SEM-XEDS confirmed that there is no recrystallized EMIM salt at the outer surface of MOF particles. This is fully consistent with the PXRD pattern of the composite, showing the absence of any Bragg peaks that can be assigned to the recrystallized EMIMCl salt. This indicates that EMIMCl is exclusively confined in the mesopores of MIL-101(Cr)–SO_3H. An EMIMCl loading of ~42 ± 5 wt% was determined by combining elemental analysis and SEM-XEDS (C, 34.7 ± 0.3 wt%; N, 9.6 ± 0.3 wt%; S, 3.2 ± 0.3 wt%; Cr, 6.5 ± 0.3 wt%; Cl, 10.5 ± 0.3 wt%). N_2 sorption isotherms revealed that the composites adsorb only a negligible amount of N_2. This is consistent with the adsorption of a large amount of EMIMCl in mesoporous cages of MIL-101(Cr)–SO_3H (Fig. 1b).

The thermal stability of EMIM@MIL-101-SO_3H was investigated using TGA coupled with Mass Spectrometry (TGA-MS) (Fig. 1c). The first weight loss is assigned to the departure of water in agreement with the increase of the Evolved Gas Analysis signal (EGA) specific to H_2O (m/z = 17 and 18). The sharp weight loss decrease observed in the [500 K–550 K] temperature range corresponds to the thermal decomposition of the incorporated EMIMCl, as shown by the characteristic fragments of the IL (m/z = 15, 29, 50, 52 and 64 for –CH_3/NH, C_2H_5, CH_3Cl from ^{35}Cl, CH_3Cl from ^{37}Cl and C_2H_5Cl from ^{35}Cl respectively, while the m/z = 66 signal assigned to C_2H_5Cl from ^{37}Cl is negligible in relation with the lower natural abundance of isotope ^{37}Cl *versus* ^{35}Cl).[60,61] Interestingly, the EMIMCl degradation occurs in the same temperature domain as that observed for the decomposition of the bulk IL (Fig. S3†). For 550 K < T < 650 K, EMIMCl degradation occurs concomitantly with that of the organic linker of the MOF, while the weight loss observed in the [650 K–750 K] temperature domain results from the complete degradation of the MOF framework. Remarkably, EMIM@MIL-101-SO_3H, exhibits a higher thermal stability (up to 500 K) than most of the previously reported IL@MOFs,[28,37,38,40] which makes this composite applicable in the target intermediate temperature domain.

To further evidence that EMIMCl is confined in the MOF pore, DSC thermogram of the bulk IL was compared to that of the composite EMIM@MIL-101-SO_3H (Fig. 1d). Upon heating from 183 K to 383 K, the bulk IL exhibits one endothermic peak around 220 K, corresponding to the glass transition ($T_{g(EMIMCl)}$), followed by the cold crystallization exothermic peak centered around 260 K.[62] The endothermic peak observed at 346 K coincides with the EMIMCl melting point.[60,61,63] In contrast, the DSC signal of EMIM@MIL-101-SO_3H shows a flat response in the whole temperature range, in line with the absence of a IL phase change due to confinement effects. This behavior is consistent with that observed for ILs confined in porous solids[28,29,64,65] and thus confirms the adsorption of IL in the MIL-101-SO_3H pores and not at the outer surface of MOF particles as also supported by PXRD and SEM-EDX analysis discussed above. It further supports that the confined EMIMCl behaves as a glassy liquid across the whole temperature range.[66] The specific electrostatic interactions between $EMIM^+$ cations and Cl^- anions in this glass-like liquid state combined with the EMIM/MOF and Cl/MOF interactions make the IL difficult to be released from the porosity compared with other single molecular guests.[29] The EMIM@MIL-101-SO_3H composite was also characterized by FT-IR spectroscopy (see Fig. S4†). The complete assignment of the main vibration bands is given in Table S2.† The FT-IR spectrum of EMIM@MIL-101-SO_3H does not show any significant shift of the vibration bands in comparison with those of the pure MOF and EMIMCl. This suggests weak van der Waals and hydrogen interactions between the two components. However, it is well known that coordinatively unsaturated Cr sites (CUS) of MIL-101(Cr) can covalently interact with N-donor ligands.[67,68] In particular, the covalent grafting of methylimidazole onto the Cr CUS of MIL-101(Cr) was previously demonstrated by combining multiple spectroscopic techniques (EPR, UV-Vis, FT-IR).[67] It can thus be assumed that the imidazole ring of EMIMCl is also covalently grafted onto the Cr site of MIL-101 (Cr)–SO_3H.

AC impedance measurements were first recorded on EMIM@MIL-101-SO_3H at the anhydrous state. The composite was preliminary *in situ* heated for 2 hours at 473 K under nitrogen flow to avoid the IL degradation, as evidenced by TGA (Fig. 2c). The real (Z') and imaginary (Z'') parts of the impedance are depicted in the Nyquist plots (Fig. S5†). With increasing the temperature, the impedance drastically decreases and the typical semi-circle profile in the low temperature domain is dominated by the capacitive tail associated with the protonic conductivity of the composite. This trend is much more pronounced than that observed for the bulk EMIMCl (Fig. S6†) and sharply contrasts with the insulating behavior of the MOF (no semi-circle profile combined with high impedance values, *e.g.* $Z > 10^{12}$ Ohm whatever T, see Fig. S7†). This observation supports a change of the MOF electrical behavior upon the adsorption of the IL, which allows the long-range transport of the H^+ issued from the –SO_3H functions of the MOF. The total impedance of EMIM@MIL-101-SO_3H was extrapolated from the low frequency end intercept of the arc on the real axis or from the linear region of the capacitive tail to the real axis, according to the Nyquist plot profile. As demonstrated,[15,69] The extrapolation procedure for analyzing Nyquist plots is perfectly suitable for determining the impedance of the system, as well as the equivalent circuits fitting approach or Bode representation. The conductivity, σ, was furthermore deduced from the formula $\sigma = 1/Z \times l/S$, where l and S are the sample thickness and area respectively. The temperature dependence of the conductivity for EMIMCl and EMIM@MIL-101-SO_3H exhibits distinct behaviors (Fig. 2a), in agreement with the typical DSC profiles of both respective solids (Fig. 1d). For bulk EMIMCl, the conductivity increase with the temperature is disrupted in the [220 K–270 K] temperature range, consistent with the glass transition and the crystallization of the IL as shown by the DSC experiments. By contrast, the conductivity of EMIM@MIL-101-SO_3H steadily rises with the temperature, in line with the absence of phase changes for the confined IL up to 473 K. The conductivity of EMIMCl in bulk phase is higher than in confined phase in the whole temperature domain, in relation with the higher vis-

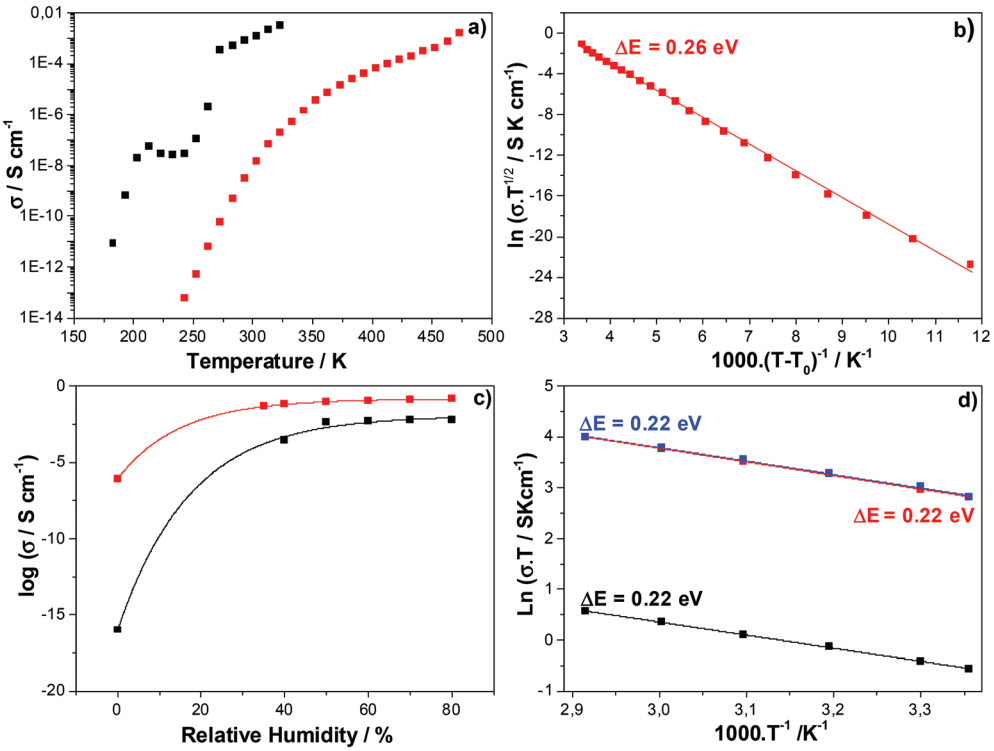

Fig. 2 (a) Temperature dependence of the conductivity for EMIMCl (black) and EMIM@MIL-101-SO_3H (red) at the anhydrous state in the temperature range of 180 K–473 K on heating, (b) VTF type plot of the conductivity for the EMIM@MIL-101-SO_3H at the anhydrous state, the solid line corresponds to the linear least-square fit, (c) humidity dependence of the conductivity recorded at 343 K for MIL-101(Cr)–SO_3H (black) and EMIM@MIL-101-SO_3H (red) in the Relative Humidity (RH) range of 0%–80%, lines are exponential fits to guide the eyes, (d) Arrhenius type plot of the conductivity for MIL-101(Cr)–SO_3H (black) and EMIM@MIL-101-SO_3H (red: cycle 1, blue: cycle 2) under 80% RH, the lines correspond to the linear least-square fit.

cosity of the system in the later case.[66] In addition, the glassy-like liquid behavior of EMIMCl confined in MIL-101(Cr)–SO_3H is evidenced by the huge decrease of the conductivity with decreasing temperature.[66] For IL localized nearby the MOF pore wall, additional structuring influences arise from the steric constraints and field effects at the interface, impacting the IL viscosity and the resulting charge carrier dynamics.[66] Moreover, the temperature dependence of the conductivity for EMIMCl@MIL-101-SO_3H shown in Fig. 2b is captured by applying the empirical Vogel–Fulcher–Tammann (VTF) equation: $\sigma T^{1/2} = \sigma_0 \exp{-[\Delta E/(k(T - T_0)]}$, where σ_0 is the conductivity at infinite temperature, k is the Boltzmann constant, ΔE corresponds to the activation energy associated with the proton transfer mechanism and $T_0 = T_{g(EMIMCl)} - 50$, with $T_{g(EMIMCl)}$ assessed by the DSC experiments (T_g = 218 K). The VTF model typically considered to describe the proton dynamics behavior of bulk ILs[63,70] was equally employed for characterizing the (EMI)[$N(CN)_2$]@PCN-777 composite.[40] The VTF model refers to the inter-relation between the protonic conductivity and the segmental relaxation of the media in which ions are moving. For EMIM@MIL-101-SO_3H, the cooperative conductivity process results from the H^+ transport assisted by the dynamics of the IL involving local motions due to their weak interactions with the MOF framework, as evidenced from IR analysis. The proton dynamics is rather restricted due to confinement effects, as stated by the higher activation energy deduced from the VTF fit parameters for EMIM@MIL-101-SO_3H (ΔE = 0.26 eV) than for bulk EMIMCl (ΔE = 0.04 eV).[70] Noteworthy, the contribution of Cl^- species to the global charge transport process cannot be completely ruled out. Most importantly, as the temperature increases, the protonic conductivity is substantially enhanced from 3.3 × 10^{-9} S cm^{-1} at 298 K to 1.5 × 10^{-3} S cm^{-1} at 473 K (see Table S3†), a level of performance comparable with the best proton conducting IL@MOF, *i.e.* EMIM@UiO-67 (σ = 1,6 × 10^{-3} S cm^{-1} at 473 K) reported so far as the sole IL@MOF composite stable in the temperature domain explored herein.[27] The comparable performance is certainly fortuitus, as UiO-67 and MIL-101(Cr)–SO_3H display different features in terms of topology, pore diameter, strength of the proton source, pore volume occupancy by EMIMCl, impacting the charge carriers density and mobility. The distinct viscosity of the ionic liquid and specific topology of the H-bonded network connecting the proton donor/acceptor sites involved in both systems are then counter-balanced, resulting in a similar conductivity value recorded at 473 K. Notably the others IL@MOF were not investigated at 473 K due to IL release or MOF degradation.[28,37,38,40] Here we demonstrate that EMIM@MIL-101-SO_3H shows struc-

tural integrity and IL retention upon heating up to 473 K, as evidenced by similar PXRD patterns (Fig. 1a) and EA data (see Table S1†), respectively before and after protonic conductivity measurements.

Impedance measurements were further recorded under humid conditions to introduce additional hydrogen-bonded charge carriers, beneficial for the charge transport. As shown in Fig. S8,† the Nyquist plots of the impedance recorded at 343 K for RH varying from 35% to 80% result from capacitive tails along with very low levels of impedance. The corresponding conductivity values show a peculiar RH dependence (see Table S3† and Fig. 2c). The conductivity substantially increases at low RH by more than 4 orders of magnitude from RH = 0% ($\sigma = 8.2 \times 10^{-7}$ S cm^{-1}) to RH = 35% ($\sigma = 4.8 \times 10^{-2}$ S cm^{-1}). Note that this sharp σ raise is likely to occur at even lower RH, but was not measurable due to equipment limitations. As previously shown for ILs[71,72] the conductivity enhancement under humidity is related to the decrease of the environment viscosity, resulting from the dissociation of the anion/cation pairs of the IL, and the solvation of ions by water molecules. With increasing RH from 35% to 80%, the conductivity increases by a factor 3 ($\sigma_{343\ K/35\%RH} = 4.8 \times 10^{-2}$ S cm^{-1} and $\sigma_{343\ K/80\%RH} = 1.4 \times 10^{-1}$ S cm^{-1}). Noteworthy this typical σ *vs.* RH profile is temperature independent, as shown by the similar trend recorded at 303 K (Fig. S9†). To explain this water-dependent protonic conductivity profile, water adsorption isotherm was recorded at 303 K (Fig. S10†). A low water uptake ($m_{ads} = 0.07$ g g^{-1}) is observed at very low relative pressure ($P/P_0 < 0.1$) since the composite shows only a limited pore accessibility to H_2O due to the high content of confined EMIMCl. However, this water amount is enough to boost the protonic conductivity of the composite observed at low RH. With increasing the relative water pressure from 10% to 80%, the water uptake exponentially rises and the adsorption and desorption branches perfectly match. Both features support that the water molecules are adsorbed at the outer-surface of the MOF in the corresponding RH domain. Assuming that all water molecules behave as charge carriers, the conductivity should follow the trend of the water uptake with increasing RH, as it is defined as $\sigma = n\mu e$, where n, μ and e are the charge carriers density, mobility and charge, respectively. On the opposite, the conductivity increment with RH is negligible compared to the exponential increase of the amount of adsorbed water molecules. This supports that the conductivity performance of the composite mainly results from the charge transport at the internal porosity of the composite, even if the contribution from the water molecules adsorbed at the outer-surface of the material cannot be totally ruled out. Fig. 2d reports the temperature-dependence of the protonic conductivity for EMIM@MIL-101-SO_3H and MIL-101(Cr)–SO_3H in the 298–343 K temperature range and RH = 80%. Both set of data follow the Arrhenius law, $\sigma T = \sigma_0 \exp - [\Delta E/(kT)]$, with comparable low activation energy (ΔE = 0.22 eV), in line with an efficient grotthus-like mechanism of the H^+ propagation since $\Delta E < 0.40$ eV, as mainly observed for water-mediated proton conducting MOFs.[11–15,73–75] As reported in other MOFs,[74,75] protons are assumed to be released from the acidic groups, *i.e.* the –SO_3H groups, towards neighboring water molecules adsorbed in the pores at low RH. They are further shuttled inside the porosity of the MOF, *via* the H-bonded network connecting –SO_3H, adsorbed water molecules, $EMIM^+$ cations and Cl^- anions species. This mechanism is assumed to remain the same at higher RH, since the composition of guests molecules, *i.e.* IL and water contents in the MOF pores, is similar all along the RH domain.[76] One notes that the chloride species solvated by water molecules are likely to contribute to the charge transport mechanism. As previously evidenced for the proton conducting MIP-202(Zr),[15] Cl^- species are able to participate to the hydrogen-bonded network resulting from the interconnection of acidic sources, water molecules and chlorine counter ions. More importantly, ΔE slightly diminishes upon hydration for EMIM@MIL-101-SO_3H (ΔE = 0.26 eV at the anhydrous state), alongside an increase of the protonic conductivity as described above. In addition, the conductivity performance is maintained after 2 cycles, corroborating the absence of any IL leaching in presence of water vapor. Indeed, the exceptional conductivity value recorded at 343 K and 80% RH ($\sigma = 1.4 \times 10^{-1}$ S cm^{-1}) is maintained over several days, in line with the long-term stability of the composite under operating conditions (Fig. S12†). Accordingly, the comparable PXRD pattern (Fig. 1a) and EA (see Table S1†) of EMIM@MIL-101-SO_3H collected before and after conductivity measurements under humidity state the structural and chemical robustness of EMIM@MIL-101-SO_3H, along with the maintained IL loading under this working condition. Such results are in line with the efficient confinement of the IL in the mesoporous cages of MIL-101-SO_3H, even in the presence of water. This is a clear advantage compared to the previously reported MIL-101(Cr)/$CaCl_2$ composites that showed a slight release of the salt.[58,59] The imidazole group of the IL is most probably covalently grafted to the Cr CUS of the MOF as it was previously demonstrated for the 1 methyl imidazole@MIL-101(Cr) by combining multiple complementary UV-vis, FT-IR and NIR spectroscopies.[67]

Remarkably, the protonic conductivity recorded at is 20 to 250-fold higher for EMIM@MIL-101-SO_3H than for MIL-101-SO_3H, for RH = 40% to 80%, respectively (see Table S3† and Fig. 2c). This reveals the synergistic role played by the water molecules and IL moieties in participating to the H^+ transport process throughout the composite. There are only a few studies on the σ–RH dependence of IL@MOFs mostly restricted to the low humidity domain. Table 1 compares the conductivity performance of EMIM@MIL-101-SO_3H with respect to other existing IL@MOF composites. At low humidity level, the conductivity of EMIM@MIL-101-SO_3H significantly surpasses that of EMIMBr@MIL-53(Al)–NH_2 by almost 3 orders of magnitude,[27] and it competes with that of [BSO_3Hmim][HSO_4]@MIL-101,[39] which was identified as the best protonic conducting IL@MOF solid reported so far at low humidity level. Interestingly, our composite outperforms by far other ternary based composites (IL/MOF/polymer), like (BMIM)BF_4/UiO-67/PAN[30] and hydroxyethyl(trimethyl) ammonium/ZIF-8/PVA.[77] At higher RH (60% < RH < 80%),

Table 1 Comparison of the protonic conductivity of EMIM@MIL-101-SO_3H and other IL@MOFs composites under low to mild humidity conditions

Composite	σ/S cm^{-1}	T/RH	Ref.
EMIMBr@MIL-53(Al)–NH_2	3.0×10^{-5}	353 K–26%	27
[BSO_3Hmim][HSO_4]@MIL-101	4.4 10^{-2}	323 K–23%	39
(BMIM)BF_4/UiO-67/PAN	2.5×10^{-4}	363 K–35%	30
Hydroxyethyl(trimethyl) ammonium@ZIF-8/PVA	9.8×10^{-4}	333 K–33%	77
EMIM@MIL-101-SO_3H	4.8×10^{-2}	343 K/35%	This work
EMIM@MIL-101-SO_3H	1.4×10^{-1}	343 K/60%–80%	This work

EMIM@MIL-101-SO_3H shows outstanding performance ($\sigma_{(343\ K/60\%-80\%RH)} \geq 10^{-1}$ S cm^{-1}) and competes with the best performing water-assisted proton conducting MOFs or coordination polymers which have been investigated at higher RH (>90%).[14,14,15,18–21,18,74,75,78–82] Propitiously, EMIM@MIL-101-SO_3H is the sole MOF-based system showing excellent protonic conductivity under moderate RH (35–40%). Decisively, our composite displays only a very small variation of σ between RH = 80% and 40%. This offers a key alternative to the water management issues, that the benchmark Nafion® based proton exchanged membranes have to face due to the membrane dehydration at $T > 353$ K.[83]

Conclusions

In summary, the impregnation of EMIMCl ionic liquid in the mesopores of MIL-101(Cr)–SO_3H was demonstrated to boost the intrinsic proton conducting performance of the parent MOF under both anhydrous and humid conditions. The good IL/MOF compatibility combined with the high chemical and thermal stability of the resulting composite led to an efficient confinement of the IL in the MOF pores up to 500 K, *i.e.* a temperature rarely explored for MOF-based composites. EMIM@MIL-101-SO_3H shows excellent protonic conductivity at 473 K (σ = 1.5 × 10^{-3} S cm^{-1}), which ranks this material amongst the best anhydrous proton conducting MOFs investigated in the intermediate temperature domain. Remarkably, this composite equally shows excellent protonic conductivity under low humidity conditions ($\sigma_{353\ K/35\%RH}$ = 4.8 × 10^{-2} S cm^{-1}), while it displays a steadily and exceptional σ(343 K) value exceeding 10^{-1} S cm^{-1} under moderate relative humidity (60% < RH < 80%). The competitive proton conducting performance of EMIM@MIL-101-SO_3H under both humid and anhydrous conditions is unprecedented and makes this composite as a promising candidate in the field of solid-state proton conductors under versatile conditions.

Author contributions

The manuscript was written through contributions of all authors. E.G. synthesized the MOF. CS.-J. and C. L. performed the FT-IR spectra and SEM-EDX experiments. N.S. analyzed the composition and microstructural characterization of composites. K.T. and S.D.-V. performed the IL impregnation and carried out the PXRD, N_2 sorption, TGA/MS, DSC, EA, water sorption and impedance data. K.T., G.M. and S.D.-V. analyzed the PXRD, N_2 sorption, TGA/MS, DSC, EA, water sorption and impedance data.

Conflicts of interest

The authors declare no competing financial interest.

Acknowledgements

TGA/MS and DSC experiments were performed with the support of the Balard Plateforme d'Analyses et de Caractérisation (PAC Balard); the authors thank Amine Geneste (PAC Balard) for technical support/assistance. Magalie Lefeuvre is acknowledged for the Elemental Analysis experiments. E.G. and N.S. acknowledge the financial support from the ANR-11-LABEX-0039 (LabEx charmmmat).

References

1 A. Kirubakaran, S. Jain and R. K. Nema, A review on fuel cell technologies and power electronic interface, *Renewable Sustainable Energy Rev.*, 2009, **13**, 2430–2440.
2 S. J. Peighambardoust, S. Rowshanzamir and M. Amjadi, Review of the proton exchange membranes for fuel cell applications, *Int. J. Hydrogen Energy*, 2010, **35**, 9349–9384.
3 P. Ramaswamy, N. E. Wong and G. K. H. Shimizu, MOFs as proton conductors – challenges and opportunities, *Chem. Soc. Rev.*, 2014, **43**(16), 5913–5932.
4 A. L. Li, Q. Gao, J. Xu and X. H. Bu, Proton-conductive metal-organic frameworks: Recent advances and perspectives, *Coord. Chem. Rev.*, 2017, **344**, 54–82.
5 X. Meng, H. N. Wang, S. Y. Song and H. J. Zhang, J. Proton-conducting, crystalline porous materials, *Chem. Soc. Rev.*, 2017, **46**, 464–480.
6 D. W. Lim, D.-W. H. Kitagawa and H. Proton, Transport in Metal–Organic Frameworks, *Chem. Rev.*, 2020, **120**, 8416–8467.
7 Y. Ye, L. Gong, S. Xiang, Z. Zhang and B. Chen, Metal–Organic Frameworks as a Versatile Platform for Proton Conductors, *Adv. Mater.*, 2020, **32**, 1907090.

8 D. W. Lim and H. Kitagawa, Rational strategies for proton-conductive metal–organic frameworks, *Chem. Soc. Rev.*, 2021, **50**, 6349–6368.
9 S. C. Pal and M. C. Das, Superprotonic Conductivity of MOFs and Other Crystalline Platforms Beyond 10^{-1} S cm^{-1}, *Adv. Funct. Mater.*, 2021, 2101584.
10 K. Biradha, A. Goswami, R. Moi and S. Saha, Metal-Organic Frameworks as Proton Conductors: Strategies for Improved Proton Conductivity, *Dalton Trans.*, 2021, **50**, 10655–10673.
11 A. Shigematsu, T. Yamada and H. Kitagawa, Control of Proton Conductivity in Porous Coordination Polymers, *J. Am. Chem. Soc.*, 2011, **133**, 2034–2036.
12 J. M. Taylor, K. W. Dawson and G. K. H. Shimizu, A Water-Stable Metal–Organic Framework with Highly Acidic Pores for Proton-Conducting Applications, *J. Am. Chem. Soc.*, 2013, **135**, 1193–1196.
13 M. Bazaga-García, R. M. P. Colodrero, M. Papadaki, P. Garczarek, J. Zoń, P. Olivera-Pastor, E. R. Losilla, L. León-Reina, M. A. G. Aranda, D. Choquesillo-Lazarte, *et al.*, Guest Molecule-Responsive Functional Calcium Phosphonate Frameworks for Tuned Proton Conductivity, *J. Am. Chem. Soc.*, 2014, **136**, 5731–5739.
14 F. Yang, G. Xu, Y. Dou, B. Wang, H. Zhang, H. Wu, W. Zhou, J. R. Li and B. Chen, A flexible metal–organic framework with a high density of sulfonic acid sites for proton conduction, *Nat. Energy*, 2017, **2**, 877–883.
15 S. Wang, M. Wahiduzzaman, L. Davis, A. Tissot, W. Shepard, J. Marrot, C. Martineau-Corcos, D. Hamdane, G. Maurin, S. Devautour-Vinot, *et al.*, A robust zirconium amino acid metal-organic framework for proton conduction, *Nat. Commun.*, 2018, **9**, 4937.
16 S. S. Nagarkar, S. M. Unni, A. Sharma, S. Kurungot and S. K. Ghosh, Two-in-one: inherent anhydrous and water-assisted high proton conduction in a 3D metal-organic framework, *Angew. Chem., Int. Ed.*, 2014, **53**, 2638–2642.
17 T. N. Tu, N. Q. Phan, T. T. Vu, H. L. Nguyen, K. E. Cordova and H. Furukawa, High proton conductivity at low relative humidity in an anionic Fe-based metal–organic framework, *J. Mater. Chem. A*, 2016, **4**, 3638–3641.
18 S. M. Elahi, S. Chand, W. H. Deng, A. Pal and M. C. Das, Polycarboxylate-Templated Coordination Polymers: Role of Templates for Superprotonic Conductivities of up to 10^{-1} S cm^{-1}, *Angew. Chem., Int. Ed.*, 2018, **57**, 6662–6666.
19 V. G. Ponomareva, K. A. Kovalenko, A. P. Chupakhin, D. N. Dybtsev, E. S. Shutova and V. P. Fedin, Imparting high proton conductivity to a metal-organic framework material by controlled acid impregnation, *J. Am. Chem. Soc.*, 2012, **134**, 15640–15643.
20 X. M. Li, L. Z. Dong, S. L. Li, G. Xu, J. Liu, F. M. Zhang, L. S. Lu and Y. Q. Lan, Synergistic Conductivity Effect in a Proton Sources-Coupled Metal–Organic Framework, *ACS Energy Lett.*, 2017, **2**, 2313–2318.
21 S. Devautour-Vinot, E. S. Sanil, A. Geneste, V. Ortiz, P. G. Yot, J. S. Chang and G. Maurin, Guest-Assisted Proton Conduction in the Sulfonic Mesoporous MIL-101 MOF, *Chem. – Asian J.*, 2019, **14**, 3561–3565.
22 X. Lai, Y. Liu, G. Yang, S. Liu, Z. Shi, Y. Lu, F. Luoa and S. Liu, Controllable proton-conducting pathways via situating polyoxometalates in targeting pores of a metal–organic framework, *J. Mater. Chem. A*, 2017, **5**, 9611–9617.
23 F. Wang, C. Liang, J. Tang, F. Zhang and F. Qu, The promotion of proton conductivity by immobilizing molybdovanadophosphoric acids in metal–organic frameworks, *New J. Chem.*, 2020, **44**, 1912–1920.
24 J. A. Hurd, R. Vaidhyanathan, V. Thangadurai, C. I. Ratcliffe, I. L. Moudrakovski and G. K. H. Shimizu, Anhydrous proton conduction at 150 °C in a crystalline metal–organic framework, *Nat. Chem.*, 2009, **1**, 705–710.
25 D. Umeyama, S. Horike, M. Inukai, Y. Hijikata and S. Kitagawa, Confinement of Mobile Histamine in Coordination Nanochannels for Fast Proton Transfer, *Angew. Chem., Int. Ed.*, 2011, **50**, 11706–11709.
26 H. B. Luo, Q. Ren, P. Wang, J. Zhang, L. Wang and X. M. Ren, High Proton Conductivity Achieved by Encapsulation of Imidazole Molecules into Proton-Conducting MOF-808, *ACS Appl. Mater. Interfaces*, 2019, **11**, 9164–9171.
27 J. Liu, X. Zou, C. Liu, K. Cai, N. Zhao, W. Zheng and G. Zhu, Ionothermal synthesis and proton-conductive properties of NH2-MIL-53 MOF nanomaterials, *CrystEngComm*, 2016, **18**, 525–528.
28 K. Fujie, K. Otsubo, R. Ikeda, T. Yamada and H. Kitagawa, Low temperature ionic conductor: ionic liquid incorporated within a metal–organic framework, *Chem. Sci.*, 2015, **6**, 4306–4310.
29 L. H. Chen, B. B. Wu, H. X. Zhao, L. S. Long and L. S. Zheng, High temperature ionic conduction mediated by ionic liquid incorporated within the metal-organic framework UiO-67(Zr), *Inorg. Chem. Commun.*, 2017, **81**, 1–4.
30 P. Chen, S. Liu, Z. Bai and Y. Liu, Enhanced ionic conductivity of ionic liquid confined in UiO-67 membrane at low humidity, *Microporous Mesoporous Mater.*, 2020, **305**, 110369–110376.
31 W. X. Chen, H. R. Xu, G. L. Zhuang, L. S. Long, R. B. Huang and L. S. Zheng, Temperature-dependent conductivity of $Emim^+$ ($Emim^+$ = 1-ethyl-3-methyl imidazolium) confined in channels of a metal–organic framework, *Chem. Commun.*, 2011, **47**, 11933–11935.
32 R. Dutta and A. Kumar, Structural and Dielectric Properties of Ionic Liquid Doped Metal Organic Framework based Polymer Electrolyte Nanocomposites, *J. Phys.: Conf. Ser.*, 2016, **765**, 012020.
33 Y. Yoshida and H. Kitagawa, Ionic Conduction in Metal–Organic Frameworks with Incorporated Ionic Liquids, *ACS Sustainable Chem. Eng.*, 2019, **7**, 70–81.
34 W. L. Xue, W. H. Deng, H. Chen, R. H. Liu, J. M. Taylor, Y. K. Li, L. Wang, Y. H. Deng, W. H. Li, Y. Y. Wen, G. E. Wang, C. Q. Wan and G. Xu, MOF-Directed Synthesis of Crystalline Ionic Liquids with Enhanced Proton Conduction, *Angew. Chem., Int. Ed.*, 2021, **60**, 1290–1297.
35 S. Shalini, T. P. Vaid and A. J. Matzger, Salt nanoconfinement in zirconium-based metal–organic frameworks leads

to pore-size and loading-dependent ionic conductivity enhancement, *Chem. Commun.*, 2020, **56**, 7245–7248.

36 X. L. Sun, W. H. Deng, H. Chen, H. L. Han, J. M. Taylor, C. Q. Wan and G. Xu, Metal–Organic Framework Impregnated with a Binary Ionic Liquid for Safe Proton Conduction above 100 °C, *Chem. – Eur. J.*, 2017, **23**, 1248–1252.

37 H. Chen, S. Y. Han, R. H. Liu, T. F. Chen, K. L. Bi, J. B. Liang, Y. H. Deng and C. Q. Wan, High conductive-long-term durable, anhydrous proton conductive solid-state electrolyte based on a metal-organic framework impregnated with binary ionic liquids: Synthesis, characteristic and effect of anion, *J. Power Sources*, 2018, **376**, 168–176.

38 Q. Xu, X. Zhang, S. Zeng, L. Bai and S. Zhang, Ionic Liquid Incorporated Metal Organic Framework for High Ionic Conductivity over Extended Temperature Range, *ACS Sustainable Chem. Eng.*, 2019, **7**, 7892–7899.

39 J. Du, G. Yu, H. Lin, P. Jie, F. Zhang, F. Qu, C. Wen, L. Feng and X. Liang, Enhanced proton conductivity of metal organic framework at low humidity by improvement in water retention, *J. Colloid Interface Sci.*, 2020, **573**, 360–369.

40 Y. Yoshida, K. Fujie, D. W. Lim, R. Ikeda and H. Kitagawa, Superionic Conduction over a Wide Temperature Range in a Metal-Organic Framework Impregnated with Ionic Liquids, *Angew. Chem., Int. Ed.*, 2019, **58**, 10909–10913.

41 K. Fujiea and H. Kitagawa, Ionic liquid transported into metal–organic frameworks, *Coord. Chem. Rev.*, 2016, **307**, 382–390.

42 F. P. Kinik, A. Uzun and S. Keskin, Ionic Liquid/Metal–Organic Framework Composites: From Synthesis to Applications, *ChemSusChem*, 2017, **10**, 2842–2863.

43 J. M. Taylor, T. Komatsu, S. Dekura, K. Otsubo, M. Takata and H. Kitagawa, The Role of a Three Dimensionally Ordered Defect Sublattice on the Acidity of a Sulfonated Metal–Organic Framework, *J. Am. Chem. Soc.*, 2015, **137**, 11498–11506.

44 S. Horike, W. Chen, T. Itakura, M. Inukai, D. Umeyama, H. Asakura and S. Kitagawa, Order-to-disorder structural transformation of a coordination polymer and its influence on proton conduction, *Chem. Commun.*, 2014, **50**, 10241–10243.

45 T. Panda, T. Kundu and R. Banerjee, Structural isomerism leading to variable proton conductivity in indium(III) isophthalic acid based frameworks, *Chem. Commun.*, 2013, **49**, 6197–6199.

46 O. Pachos, J. Kunze, U. Stimming and F. Maglia, A review on phosphate based, solid state protonic conductors for intermediate temperature fuel cells, *J. Phys.: Condens. Matter*, 2011, **23**, 234110.

47 Y. Huang, Q. Li, A. H. Jensen, M. Yin, J. O. Jensen, E. Christensen, C. Pan, N. J. Bjerrum and W. Xing, Niobium phosphates as an intermediate temperature proton conducting electrolyte for fuell cells, *J. Mater. Chem.*, 2012, **22**, 22452–22458.

48 T. Xiao, R. Wang, Z. Chang, Z. Fang, Z. Zhu and C. Xu, Electrolyte membranes for intermediate temperature proton exchange membrane fuel cell, *Prog. Nat. Sci.: Mater. Int.*, 2020, **30**, 743–750.

49 A. A. Lysova and A. B. Yaroslavtsev, New proton-conducting membranes based on phosphorylated polybenzimisazole and silica, *Inorg. Mater.*, 2019, **55**, 470–476.

50 P. Wasserscheid and T. Welton, in *Ionic Liquids in Synthesis*, Wiley-VCH Verlag, Weinheim, 2003.

51 A. Singh, R. Vedarajan and N. Matsumia, Modified Metal Organic Frameworks (MOFs)/Ionic Liquid Matrices for Efficient Charge Storage, *J. Electrochem. Soc.*, 2017, **164**, H5169–H5174.

52 Z. Wang, H. Zhou, C. Meng, W. Xiong, Y. Cai, P. Hu, H. Pang and A. Yuan, Enhancing Ion Transport: Function of Ionic Liquid Decorated MOFs in Polymer Electrolytes for All-Solid-State Lithium Batteries, *ACS Appl. Energy Mater.*, 2020, **3**, 4265–4274.

53 J. M. Tuffnell, J. K. Morzy, R. Tan, Q. Song, C. Ducati, T. D. Bennett and S. E. Dutton, Comparison of the ionic conductivity properties of microporous and mesoporous MOFs infiltrated with a Na-ion containing IL mixture, *Dalton Trans.*, 2020, **49**, 15914–15924.

54 M. Benzaqui, R. Semino, F. Carn, S. Rodrigues Tavares, N. Menguy, M. Giménez-Marqués, E. Bellido, P. Horcajada, T. Berthelot, A. I. Kuzminova, *et al.*, Covalent and Selective Grafting of Polyethylene Glycol Brushes at the Surface of ZIF-8 for the Processing of Membranes for Pervaporation, *ACS Sustainable Chem. Eng.*, 2019, **7**, 6629–6639.

55 H. Zhang, J. James, M. Zhao, Y. Yao, Y. Zhang, B. Zhang and Y. S. Lin, Improving hydrostability of ZIF-8 membranes via surface ligand exchange, *J. Membr. Sci.*, 2017, **532**, 1–8.

56 K. Wang, H. Huang, X. Zhou, Q. Wang, G. Li, H. Shen, Y. She and C. Zhong, Highly Chemically Stable MOFs with Trifluoromethyl Groups: Effect of Position of Trifluoromethyl Groups on Chemical Stability, *Inorg. Chem.*, 2019, **58**, 5725–5732.

57 E. Gkaniatsou, R. Ricoux, K. Kariyawasam, I. Stenger, B. Fan, N. Ayoub, S. Salas, G. Patriarche, C. Serre, J.-P. Mahy, *et al.*, Encapsulation of Microperoxidase-8 in MIL-101(Cr)-X Nanoparticles: Influence of Metal–Organic Framework Functionalization on Enzymatic Immobilization and Catalytic Activity, *ACS Appl. Nano Mater.*, 2020, **3**, 3233–3243.

58 A. Permyakova, S. Wang, E. Courbon, F. Nouar, N. Heymans, P. D'Ans, N. Barrier, P. Billemont, G. De Weireld, N. Steunou, *et al.*, Design of salt–metal organic framework composites for seasonal heat storage applications, *J. Mater. Chem. A*, 2017, **5**, 12889–12898.

59 P. D'Ans, E. Courbon, A. Permyakova, F. Nouar, C. Simonnet-Jégat, F. Bourdreux, L. Malet, C. Serre, M. Frère and N. Steunou, A new strontium bromide MOF composite with improved performance for solar energy storage application, *J. Energy Storage*, 2019, **25**, 100881.

60 A. Efimova, G. Hubrig and P. Schmidt, Thermal stability and crystallization behavior of imidazolium halide ionic liquids, *Thermochim. Acta*, 2013, **573**, 162–160.

61 A. Efimova, L. Pfützner and P. Schmidt, Thermal stability and decomposition mechanism of 1-ethyl-3-methyl-

imidazolium halidesP., *Thermochim. Acta*, 2015, **604**, 129–136.
62 E. Goomez, N. Calvar and A. Domínguez, in *Current state of the art, Chap. 8: Thermal behaviour of pure ionic liquids*, 2015, pp. 199–228.
63 F. Liu, X. Zhong, J. Xu, A. Kamali and Z. Shi, Temperature Dependence on DensityViscosity, and Electrical Conductivity of Ionic Liquid 1-Ethyl-3-Methylimidazolium Fluoride, . *Appl. Sci.*, 2018, **8**, 356–364.
64 K. Fujie, T. Yamada, R. Ikeda, H. Kitagawa and H. Introduction, of an Ionic Liquid into the Micropores of a Metal–Organic Framework and Its Anomalous Phase Behavior, *Angew. Chem., Int. Ed.*, 2014, **53**, 11302–11305.
65 Y. Xin, C. Wang, Y. Wang, J. Sun and Y. Gao, Encapsulation of an ionic liquid into the nanopores of a 3D covalent organic framework, *RSC Adv.*, 2017, **7**, 1697–1700.
66 S. Marion, S. J. Davis, Z.-Q. Wu and A. Radenovic, Nanocapillary confinement of imidazolium based ionic liquids, *Nanoscale*, 2020, **12**, 8867–8874.
67 W. R. Webb, M. E. Potter, D. J. Stewart, S. J. Elliott, P. J. A. Sazio, Z. Zhang, H. K. Luo, J. Teng, L. Zhang, C. Ivaldi, *et al.*, The Significance of Metal Coordination in Imidazole-Functionalized Metal–Organic Frameworks for Carbon Dioxide Utilization, *Chem. – Eur. J.*, 2020, **26**, 13606–13610.
68 Y. K. Hwang, D.-Y. Hong, J.-S. Chang, S. H. Jhung, Y.-K. Seo, J. Kim, A. Vimont, M. Daturi, C. Serre and G. Férey, Amine Grafting on Coordinatively Unsaturated Metal Centers of MOFs: Consequences for Catalysis and Metal Encapsulation, *Angew. Chem., Int. Ed.*, 2008, **120**, 4212–4216.
69 M. Wahiduzzaman, S. Nandi, V. Yadav, K. Taksande, G. Maurin, H. Chun and S. Devautour-Vinot, Superionic conduction in a zirconium-formate molecular solid, *J. Mater. Chem. A*, 2020, **8**, 17951–17955.
70 J. Vila, C. Franjo, J. M. Pico, L. M. Varela and O. Cabeza, Temperature Behavior of the Electrical Conductivity of Emim-Based Ionic Liquids in Liquid and Solid States, *Port. Electrochim. Acta*, 2007, **25**, 163–172.
71 W. Silva, M. Zanatta, A. S. Ferreira, M. C. Corvo and E. J. Cabrita, Revisiting Ionic Liquid Structure-Property Relationship: A Critical Analysis, *Int. J. Mol. Sci.*, 2020, **21**, 7745–7782.
72 J. Jacquemin, P. Husson, A. A. H. Padua and V. Majer, Density and viscosity of several pure and water-saturated ionic liquids, *Green Chem.*, 2006, **8**, 172–180.
73 C. J. T. de Grotthuss, Sur la décomposition de l'eau et des corps qu'elle tient en dissolution à l'aide de l'électricité galvanique, *Ann. Chim.*, 1806, **58**, 54–73.
74 M. Wahiduzzaman, S. Wang, J. Schnee, A. Vimont, V. Ortiz, P. G. Yot, R. Retoux, M. Daturi, C. Serre, G. Maurin and S. Devautour-Vinot, A High Proton Conductive Hydrogen-Sulfate Decorated Titanium Carboxylate Metal–Organic Framework, *ACS Sustainable Chem. Eng.*, 2019, **7**, 5776–5783.
75 S. Nandi, S. Wang, M. Wahiduzzaman, V. Yadav, K. Taksande, G. Maurin, C. Serre and S. Devautour-Vinot, Multivariate Sulfonic-Based Titanium Metal–Organic Frameworks as Super-protonic Conductors, *ACS Appl. Mater. Interfaces*, 2021, **13**, 20194–20200.
76 S. Tominaka and A. K. Cheetham, Intrinsic and extrinsic proton conductivity in metal-organic frameworks, *RSC Adv.*, 2014, **4**, 54382–54387.
77 C. Liu, S. Feng, Z. Zhuang, D. Qi, G. Li, C. Zhao, X. Li and H. Na, Towards basic ionic liquid-based hybrid membranes as hydroxide-conducting electrolytes under low humidity conditions, *Chem. Commun.*, 2015, **51**, 12629–12632.
78 S. Mukhopadhyay, J. Debgupta, C. Singh, R. Sarkar, O. Basu and S. K. Das, Designing UiO-66-Based Superprotonic Conductor with the Highest Metal–Organic Framework Based Proton Conductivity, *ACS Appl. Mater. Interfaces*, 2019, **11**, 13423–13432.
79 Y. Y. Cai, Q. Yang, Z. Y. Zhu, Q. H. Sun, A. M. Zhu, Q. G. Zhang and Q. L. Liu, Achieving efficient proton conduction in a MOF-based proton exchange membrane through an encapsulation strategy, *J. Membr. Sci.*, 2019, **590**, 117277.
80 X. M. Li, J. Liu, C. Zhao, J. L. Zhou, L. Zhao, S. L. Lia and Y. Q. Lan, Strategic hierarchical improvement of superprotonic conductivity in a stable metal–organic framework system, *J. Mater. Chem. A*, 2019, **7**, 25165–25171.
81 R. F. Mendes, P. Barbosa, E. M. Domingues, P. Silva, F. Figueiredo and F. A. Almeida Paz, Enhanced proton conductivity in a layered coordination polymer, *Chem. Sci.*, 2020, **11**, 6305–6311.
82 S. S. Liu, Z. Han, J. S. Yang, S. Z. Huang, X. Y. Dong and S. Q. Zang, Sulfonic Groups Lined along Channels of Metal–Organic Frameworks (MOFs) for Super-Proton Conductor, *Inorg. Chem.*, 2020, **59**(1), 396–402.
83 H. Zhang and P. K. Shen, Recent Development of Polymer Electrolyte Membranes for Fuel Cells, *Chem. Rev.*, 2012, **112**, 2780–2832.